BIOMASS END-TO-END PERFORMANCE SIMULATOR: DESCRIPTION OF THE IONOSPHERE MODULE

A. Camps[1], J. Barbosa[2], I. Nestoras[2], A. Jordão[2], M. J. Sanjuan-Ferrer[3], M. Rodriguez-Cassola[3]
[1]CommSensLab-UPC Unidad María de Maeztu – Dep. of Signal Theory and Communications, and IEEC/CTE-UPC, Universitat Politècnica de Catalunya - Campus Nord, E-08034 Barcelona, Spain
[2]RDA - Research and Development in Aerospace GmbH, Zürich, Switzerland
[3]German Aeospace Center (DLR), DLR Microwaves and Radar Institute, Oberpfaffenhofen, 82234 Weßling, Germany
E-mail: camps@tsc.upc.edu

ABSTRACT

ESA's BIOMASS Earth Explorer mission aims at providing global above ground forest biomass. Its payload is a UHF synthetic aperture radar. At UHF ionospheric effects, notably the group delay and phase advance, the Faraday rotation, and the intensity and phase scintillations (or rapid fluctuations) are significant and have to be properly modelled to be compensated, to understand the limitations of the proposed technique, and to select the optimum observation conditions. This paper summarizes the structure and main characteristics of the ionospheric module of the BIOMASS end-to-end performance simulator (BEEPS-IOM).

Index Terms— SAR UHF, ionosphere, Faraday rotation, delay, phase, intensity, scintillation.

1. INTRODUCTION

ESA's BIOMASS is the seventh Earth Explorer mission [1]. It aims at providing global above ground forest biomass and biomass change maps of ≤20% accuracy, 100-200 m spatial resolution, and 6-12 months temporal resolution; global forest disturbance maps of ≥ 90% classification accuracy, 50-200 m spatial resolution, and 2-12 months temporal resolution; and global forest height maps of 20-30% accuracy, 100 m spatial resolution, and 12 months temporal resolution.

BIOMASS is based on a P-band SAR (438 MHz) orbiting in a dawn-dusk, Sun-synchronous orbit at 674 km, that will systematically acquire fully- (quad-) polarized image data in an interferometric mode over all major forested areas on the globe and a tomographic phase (7 images) to retrieve forest vertical structure information. The inversion methodology is then based on backscatter intensity measurements at different polarizations and interferometric coherence measurements at different polarizations.

Ionospheric effects at P-band are very important and need to be corrected for. Within the activities of the BIOMASS End-to-End Performance Simulator (BEEPS) an Ionospheric Module (IOM) is being developed by IEEC/UPC (ES) and RDA (CH).

2. MAIN IONOSPHERIC DISTURBANCES

The main disturbances experienced by a radio signal passing through the ionosphere are the Faraday rotation, the group delay and phase advance, the amplitude and phase scintillations and the refraction and wave dispersion, which are briefly described below:

- When transmitting a linearly polarized wave (BIOMASS case), Faraday rotation induces a change in the polarization plane that mixes the vertical and horizontal polarizations, thus degrading the polarization purity.

$$\theta_{Faraday} = \frac{2.36\times10^{-14}}{f^2}\sum_i B_i \cdot STEC_i \cos(\theta_i)\,, \qquad (1)$$

where $\theta_{Faraday}$ is the angle of rotation [rad], B_i is the average Earth's magnetic field in a layer i [Teslas], f is the frequency [GHz], $STEC_i$ is the Slant Total Electron Content in [e$^-$/m^2] in a layer i, and θ_i is the look angle (note subscript is kept to include potential bending of the angle due to small variations of the index of refraction). Faraday rotation cannot be predicted as it depends in many different factors, including geographic coordinates, local time, season and Solar activity. Intense and fast variations of the Faraday rotation angle in VHF-UHF signals have been associated with strong and fast amplitude scintillations, notably at equatorial latitudes.

- Group delay is the time delay in excess of the propagation time in free space. In the same way, the phase is advanced by the same amount. The group delay [s] can be computed as:

$$t = 1.345\ STEC/f^2 \times 10^{-7}, \qquad (2)$$

- Systems involving wideband transmissions at VHF and possibly UHF must also take dispersion into account [2], as for TEC = $5 \cdot 10^{17}$ e$^-$/m^2, a signal with a pulse width of 1 μs will experience a differential delay of ~0.02 μs at 200 MHz while at 600 MHz the delay would be ~0.00074 μs.
- Localized irregularities in the ionosphere TEC act as convergent and divergent lenses focusing and defocusing electromagnetic waves. These effects are called scintillations and affect the intensity, phase, and angle-of-arrival of the signal. The intensity of the scintillations is characterized by the scintillation index (S_4) defined as:

$$S_4 = \sqrt{\frac{\langle I^2\rangle - \langle I\rangle^2}{\langle I\rangle^2}}, \qquad (3)$$

 DOI 10.1109/IGARSS47720.2021.9554570

being I the intensity of the signal, and by σ_ϕ, the standard deviation of the phase fluctuations, computed over a given period of time. Apart from intensity scintillations, average ionospheric attenuation is negligible at UHF frequencies, as it is less than 0.1 dB even at very large elevation angles.

Of course, these effects affect twice the radio wave as it propagates from the radar antenna to the target (pixel over the Earth's surface), and scatters back to the antenna. According to [3], for a monostatic radar, the two-way S_4 and σ_ϕ can be computed from its correspondence of one-way scintillation index (S_4^{1w}) and one-way standard deviation of the phase fluctuations (σ_ϕ^{1w}) as:

$$S_4 = S_4^{1w} \cdot \sqrt{\frac{4+6\cdot\left(S_4^{1w}\right)^2}{1+\left(S_4^{1w}\right)^2}}, \quad (4)$$

$$\sigma_\phi = 2 \cdot \sigma_\phi^{1w}. \quad (5)$$

3. IONOSPHERIC MODELLING

Figure 1 below presents the block diagram of the Ionospheric Module being implemented for BEEPS. Cylinders represent the external input parameters, brown boxes the APIs and main algorithms, yellow boxes the high-level modules, and the orange rhomboids the external interfaces.

- **Background TEC** data can be derived from:
  - The International Reference Ionosphere (IRI) model [4] or NeQuick [5]. Vertical Total Electron Content (VTEC) can be computed from the electron density Ne [m^{-3}] as a function of height.
  - IONEX files [6] provide VTEC maps with spatial resolution of 5° in longitude, 2.5° in latitude, every 2 h.
  - GNSS Total Electron Content data exchange format (GTEX) [6].
  - GIM - GPS Total Electron Content (TEC) produced by the International Global Navigation Satellite Systems Service (IGS) Ionosphere Working Group.
  - Near Real Time VTEC data provided by DLR at an equivalent shell-height of 400 km.
- **TEC Stochastic Variability** Model (b1) consists of random variations over the background value computed as a mean value plus a uniform random variable computed from LUTs (Look Up Tables) that use the year, month, and local time, and latitude as input variables [7]. These LUTs have been derived by the gAGE/UPC group after a comprehensive analysis of the VTEC Global Ionospheric Maps ("Final Products"), published by the International GNSS Service (IGS), from 2001 to 2015 over a 20°×20° grid.
- **Bubbles and Depletions** Modelling (b2) includes an analytical model for slow refractive scintillation [7]. Refractive ionospheric effects include the ionospheric depletions and bubbles (EPBs) in equatorial regions (low frequency TEC fluctuations), and the high frequency TEC fluctuations at high latitudes for which $\sigma_\phi \neq 0$, despite $S_4 \approx 0$.

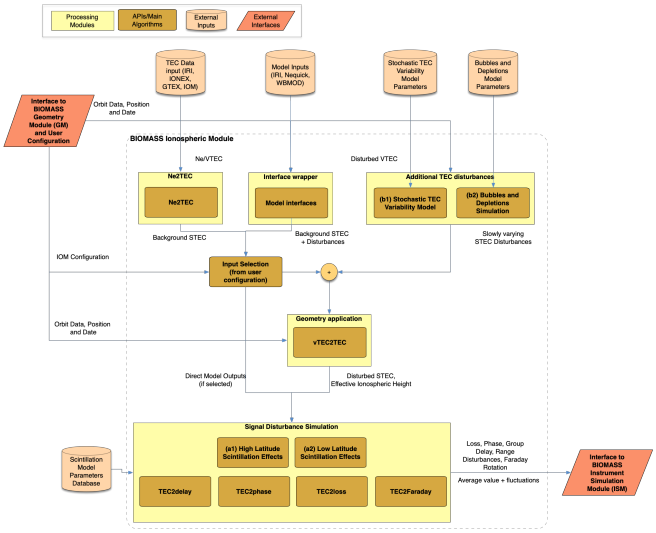

Figure 1. Block diagram of the Ionospheric Module simulator

Low-frequency TEC variations are modelled based on the available EPBs model parameters derived from a comprehensive analysis performed by the Observatori de l'Ebre, which include the EPB depth (ΔSTEC) and the size (in terms of the duration and area of the depletion itself), both depending on local time, season and year. The speed vector defined as a modulus and "azimuth" direction: $|\vec{v}| \approx 100\,m/s$, and $arg\,(\vec{v}) \approx \pm 30°$, depending on the hemisphere have been considered also. EPBs are assumed to have a Gaussian shape to provide a continuous variation of the STEC. All these parameters are random variables with geographical and temporal dependences.

At this point the VTEC is converted into the Slant TEC (STEC) using the mapping function:

$$M = \frac{1}{\sqrt{1-\left(\frac{R_E \cdot cos(\theta_{elev})}{R_E+h_{iono}}\right)^2}}, \quad (6)$$

where θ_{elev} is the elevation angle, R_E the Earth radius, and h_{iono} the height of the ionospheric height assumed as a thin shell.

- **Fast scintillations** are implemented using Rino's multiple phase screen scintillation model [8]. It requires as input variables: the ionospheric pierce point height, the frequency, the receiver and transmitter (or transmitter and scattering point) latitude, longitude and altitude, the date and Universal Time (hh:mm), the geometric enhancement factor or asymmetry of the ionospheric irregularities (a/b, with a and b the principal and secondary anisotropy elongation factors), the thickness of the scattering layer l_p, which can be divided in N slabs of l_p/N thickness each, the spectral index parameter for each power-law segment (ν_1, ν_2), which transition at a wavenumber equal to $q_L = 2\pi/l_L$, the integrated strength of the turbulence at 1 km scale (C_kL), which is related to C_s the power-law turbulent strength parameter of the spectrum of turbulences, and the effective velocity (v_{eff}).

A task still to be conducted in the frame of the project is the connection between the above physically-based parameters in Rino's model, and the (one way) S_4 and σ_ϕ values produced by ionospheric scintillation models such as GISM, WBMOD, COSMIC, ESA's SCIONAV model for σ_ϕ [7], or the modified COSMIC model as proposed in the frame of ESA's CLIMIONO project [9] for S_4.

From the analysis conducted, it seems that GISM tends to overestimate S_4 and σ_ϕ, while WBMOD seems to be more realistic reproducing the diurnal scintillation variations. However, none of them seem capable to reproduce the patchy character of the equatorial scintillation, as they just predict the average scintillation behavior as a function of time and position, and for most of the time, they fail to predict the scintillation on a given GPS link. SCIONAV attempted to fix this by adding the bubbles and depletions contributions, and improved the high latitude model of σ_ϕ. Additionally, in CLIMIONO the modified COSMIC model significantly improved the statistics of the observed S_4 for all regions. The best results are shown in Figs. 2 and 3. One limitation though, is that SCIONAV and COSMIC models were derived at L1 frequency, so they will have to be scaled at UHF using the actual frequency dependence. The weak scintillation theory for a power-law spectrum predicts a scintillation index (X = S_4 or σ_ϕ) with frequency dependence given by [10]:

$$\frac{X_{f_1}}{X_{f_2}} \propto \left(\frac{f_2}{f_1}\right)^{\frac{p+2}{4}}, \qquad (7)$$

where f_i is the frequency, the subscripts refer to the carrier frequencies, and (p+2)/4 is the spectral index.

- Last, **Faraday rotation**, **group delay** and **phase advance**, and dispersion are computed using eqns. 1 and 2. **Ionospheric losses** above VHF are very small. The one-way absorption has an average value of ~0.010 dB at mid-latitudes for a zenith path. At polar and auroral regions the average absorption is ~0.045 dB for zenith path [RD38]. From 45° to 65° latitude a linear transition is proposed.

BEEPS-IOM includes **three temporal scales** for the different phenomena in the ionosphere: slow and fast scintillations, and a medium scale to account for the movement of the bubbles and depletions, and the spacecraft over the ionospheric "screen":

- The slow variations are due to the varying evolution of the STEC (Slant Total Electron Content) over time, and geographically, and can be assumed to be constant for the whole simulation period. The same thing happens for the stochastic variability added on top of the STEC.
- The medium scale corresponds to the movement of the bubbles and depletions (~100 m/s), so in a long simulation (up to 17 min), they can travel ~100 km, which is comparable to BIOMASS swath (3 x 50 km).
- The fast scale is due to the refractive and diffractive scintillations, which are characterized by either S_4 and σ_ϕ, and the slope of the spectrum (p).

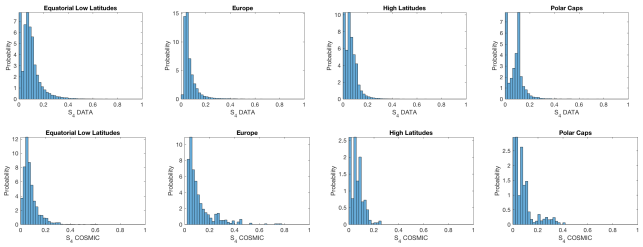

Figure 2. (top) S_4 PDF, from the ground measurements, and (bottom) from SCIONAV+COSMIC model, per region.

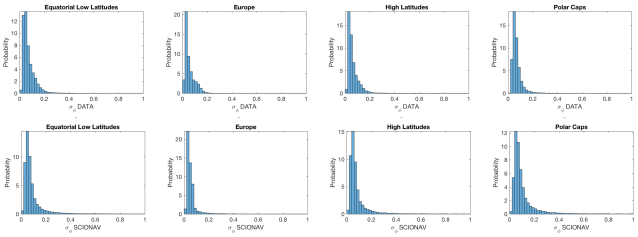

Figure 3. (top) σ_ϕ PDF, from the ground measurements, and (bottom) from SCIONAV+COSMIC model, per region.

4. SIMULATION RESULTS

Figures 4, 5 and 6 illustrate the BEEPS-IOM simulator sample outputs. Figure 4 describes the geometry of observation for one "snap-shot": black square on the Earth's surface, and blue square as intercepted in the ionosphere, from the S/C in the positions indicated by the red circle. Figure 5 shows some sample results corresponding to the first snap-shot: the STEC (bubbles and depletions not activated in this run), total Earth's magnetic field, absorption, and the Faraday rotation. Figure 6 shows the phase (left) and intensity (right) scintillation "masks" for $C_kL = 10^{30}$ (low scintillation) and 10^{33} (strong scintillation). These "masks" account for the fast intensity and phase fluctuations, and 1) are displaced in space following the iso-magnetic field lines at ~100 m/s, and 2) have a correlation time τ_c, so even for the same latitude-longitude pixel these effects vary over time.

5. CONCLUSIONS AND FUTURE WORK

The key features of the BEEPS-IOM have been presented, as well as the approach to model the background ionospheric TEC, with its stochastic variability and EPBs.

Fast scintillations are based on the solution of the forward propagation equation (FPE) assuming a phase screen (thin layer) at a constant height. Presented results have been cross-validated with existing models and tools, and a strategy is presented for the fast scintillations, to include the ionospheric drift, and the satellite movement. Future work will target to find a relationship between S_4, σ_ϕ and the slope of the phase spectra, with the parameters in Rino's model (C_kL, a/b, l_p, number of slabs, ν_1 and ν_2, $q_L=2\pi/l_L$, v_{eff} etc. or find auxiliary sources of information for these variables.

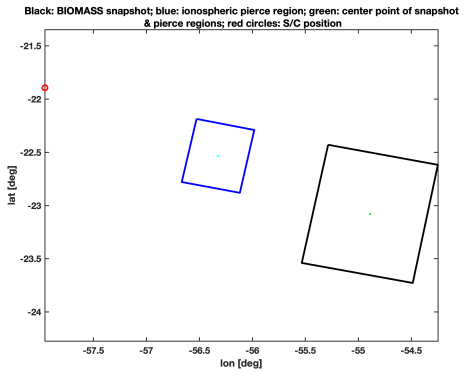

Figure 4. Sample snap shot acquisition: black square represents the BIOMASS snapshot on the Earth's surface, blue square the intercepted ionosphere region corresponding to the black square, red circle corresponds to the S/C position, and green dots the center of each snap shot on the ground or in the ionosphere.

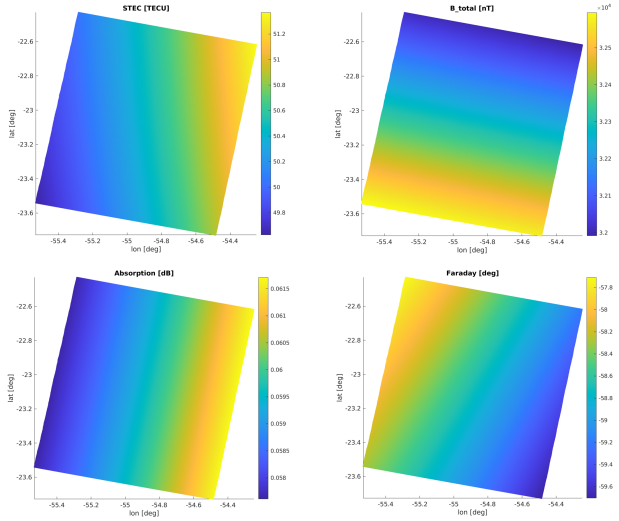

Figure 5. Sample simulator outputs for the first "snap-shot" in Fig. 4 (bottom): STEC, total magnetic field, absorption, and Faraday rotation.

6. ACKNOWLEDGMENTS

This work was supported by ESA/ESTEC project (DLR sub-contract Nr. D/551/67282068) "BIOMASS Ionospheric Module for End-to-End Performance Simulator," by the Spanish Ministry of Science, Innovation and Universities, "Sensing with Pioneering Opportunistic Techniques," grant RTI2018-099008-BC21/AEI/10.13039/501100011033, and by the Unidad de Excelencia Maria de Maeztu MDM-2016-0600.

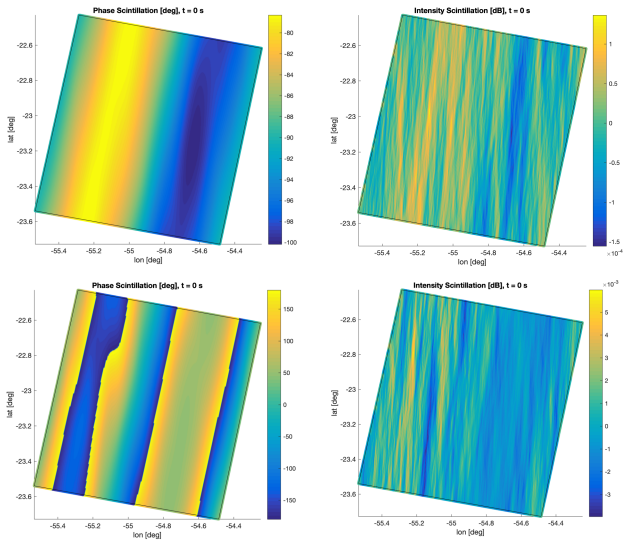

Figure 6. Sample simulation results for the snap-shot in Fig. 4, for phase (left column) and intensity (right column). Parameters used: $C_kL = 10^{30}$ (top row) and $C_kL = 10^{33}$ (bottom row), $l_{outer} = 100$ km, $l_p = 250$ m (layer thickness), $q_L = 2\pi / l_{outer}$, $\nu_1=\nu_2=2.65$, $a = 10$, and $b = 1$.

7. REFERENCES

[1] ESA BIOMASS Mission: https://directory.eoportal.org/web/eoportal/satellite-missions/b/biomass (last visited January 2021)

[2] Transionospheric radio propagation: The Global Ionospheric Scintillation Model (GISM) https://www.itu.int/pub/R-REP-P.2097-2007 (last visited January 2021)

[3] X. Pi and S. Chan, Effects of Polar Ionospheric Scintillation on L-Band Space-Based Radar, JPL-CalTech Tech Rpt, 2-10-06

[4] International Reference Ionosphere model: http://irimodel.org/ (last visited January 2021)

[5] NeQuick model: https://t-ict4d.ictp.it/nequick2 (last visited January 2021)

[6] M. Ishii, "Formats and Standards. A new GNSS Total Electron Content data exchange format (GTEX)," WMO ICTSW-4/Doc.8.2(2) REV1 (28.XI. 2013).

[7] A. Camps et al., "Improved modelling of ionospheric disturbances for remote sensing and navigation," 2017 IEEE International Geoscience and Remote Sensing Symposium (IGARSS), Fort Worth, TX, 2017, pp. 2682-2685, doi: 10.1109/IGARSS.2017.8127548.

[8] C. Rino, "The Theory of Scintillation with Applications in Remote Sensing," ed. Wiley-IEEE Press, 2011 [Chapter 4 and Appendix 2]

[9] A. Camps, G. Gonzalez-Casado, J.M. Juan, H. Park, J. Barbosa, Ionospheric Scintillation Model Limitations and Impact in GNSS-R Missions, 2020 IEEE International Geoscience and Remote Sensing Symposium (IGARSS), virtual symposium, 2020

[10] R.K. Crane, "Morphology of Ionospheric Scintillation," MIT-Lincoln Labs, TN 1974-29, 21/ May 1974